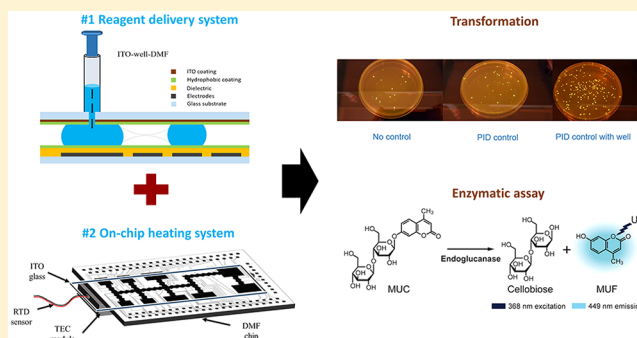


Integration of World-to-Chip Interfaces with Digital Microfluidics for Bacterial Transformation and Enzymatic Assays

Ehsan Moazami,^{†,‡} James M. Perry,^{‡,§} Guy Soffer,^{†,‡} Mathieu C. Husser,^{‡,§} and Steve C. C. Shih^{*,†,‡,§}[†]Department of Electrical and Computer Engineering, Concordia University, Montréal, Québec H3G1M8, Canada[‡]Centre for Applied Synthetic Biology, Concordia University, Montréal, Québec H4B1R6, Canada[§]Department of Biology, Concordia University, Montréal, Québec H4B1R6, Canada

Supporting Information

ABSTRACT: Digital microfluidics (DMF) represents an alternative to the conventional microfluidic paradigm of transporting fluids in enclosed channels. One of the major benefits of DMF is that fluid motion and control is achieved without external pumps. The automation component of DMF have pushed the barriers of this “lab-on-chip” technology. However, integration with external components (i.e., “world-to-chip”) interfaces have been a challenge. Two common “world-to-chip” challenges are (1) delivering biological samples to DMF devices and (2) accurately controlling temperatures on device. To address these challenges, this work describes two “world-to-chip” interface features that have been integrated on a DMF platform: a reagent delivery system and a thermal control apparatus. This platform enables a variety of biological or chemical experiments to be conducted on-chip while reducing manual intervention. Specifically, our platform increases reagent volumes available to device reservoirs volume by at least 50-fold eliminating the need to manually refill reservoirs while improving droplet dispensing reproducibility. In addition, we have integrated a closed-loop temperature control system that offers precise temperature control on-chip. To validate our “world-to-chip” interface, we have automated bacterial transformation and enzymatic assay protocols, showing that such a system enhances DMF performance. Overall, we propose that this system will improve biological experimentation which requires fluidic and temperature control integrated on DMF platforms.



Microfluidics is a valued liquid handling tool for biological and chemical assays. The advantages of low reagent consumption and automation is particularly useful for point-of-care diagnostics, cell-based assays for drug discovery, and immuno-based enzymatic assays.^{1–3} Recently, digital microfluidics (DMF) have emerged as a platform to manipulate droplets without the need for pumps, moving parts, or valves. Droplets on DMF devices are individually addressable using an electrostatic force that allows for a number of fluidic operations, such as splitting, merging and mixing to be performed on the device—a great advantage over other microfluidics paradigms. Given these functionalities, DMF platforms have been developed to automate magnetic-bead based immunoassays,⁴ cell-based assays,^{5,6} as well as tackle the workflows of synthetic biology including DNA assembly and transformation.^{7,8} Despite the attractive capabilities of DMF, a reoccurring issue lies in “world-to-chip” interfacing. Typically, “world-to-chip” interfacing accounts for fluidic interconnects, that is, to deliver fluids from the macro-world to the micro-device. Here, we consider “world-to-chip” to be any external component that interfaces with the device that will enable facile automated operations on the device and minimize manual intervention. Hence, in this work, we deliver samples

between device and user, as well as provide the appropriate thermal conditions for a given biological reaction on a DMF device.

Temperature control is critical for many biological protocols namely, polymerase chain reaction (PCR) and protein crystallization,^{9–11} as well as heat-shock transformation.¹² The vast majority of studies requiring temperature control use hot-plates, water baths, or thermal cyclers. These systems facilitate both homogeneous temperature regulation and linear temperature profiles, often with a high degree of accuracy. However, since these systems are not designed with the specifications of DMF in-mind they pose a limited degree of effectiveness when used with DMF. There are studies which report strategies to incorporate thermal electric coolers (TEC) for synthetic biology applications,⁸ but these studies do not incorporate closed-loop control. In fact, closed-loop control requires gain-tuning processes to achieve steady-state output. This tuning process can be difficult for users not familiar with control theory and therefore it is a persistent roadblock

Received: December 14, 2018

Accepted: March 19, 2019

Published: April 4, 2019

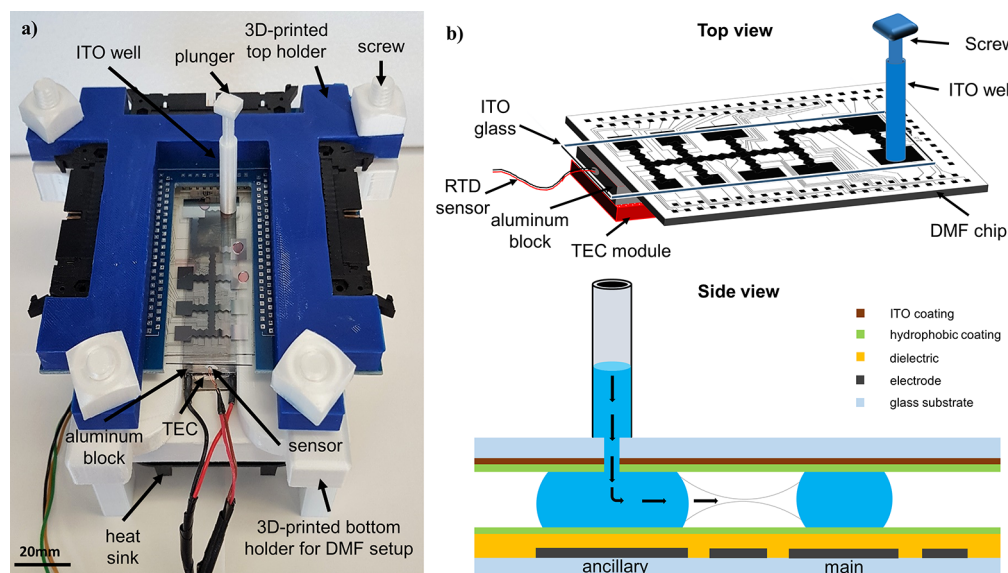


Figure 1. “World-to-chip” interfaces for digital microfluidics. (a) DMF device integrated with world-to-chip interface. Two world-to-chip interfaces are shown: (1) a reagent delivery system with a 3D printed screw and (2) a thermoelectric cooler (TEC). The device is held in-place between a 3D printed holder with connectors that interface to the automation system. (b) A top view schematic showing a ITO-well-DMF setup. A side view schematic showing the delivery of the fluid from the 3D printed well to the reservoir on the DMF device.

preventing wide adoption of this technique. To the best of our knowledge, a closed-loop system for controlling TEC with digital microfluidics have not been developed.

The second limitation for DMF (and possibly for all microfluidic systems) is the development of fluidic interfaces for delivering liquids. It is notoriously difficult to continuously deliver reagents to the reservoirs for continuous and repetitive dispensing, especially for long-term device usage and to store a large volume ($>10 \mu\text{L}$). In previous work, off-chip pressure sources are used to dispense liquids directly to a DMF device reservoir.^{12,13} Another option is to preload dried reagents and rehydrate them as they are needed instead of repetitive dispensing.¹⁴ Currently, a popular technique to improve “world-to-chip” interfaces is the use of fluidic connector components fabricated using 3D printers. 3D printing provides a convenient one-step manufacturing approach for fabricating microfluidic devices^{15,16} and greatly expands the options available to solve “world-to-chip” interfacing. In fact, for microchannel-based techniques, 3D printed fluidic port connectors (or valves) store and deliver reagents to the fluidic channels.^{17,18} Despite wide use of 3D printed connector components in microfluidics, its use have been limited in DMF.

In response to “world-to-chip” interface challenges associated with digital microfluidics, we have developed a new strategy to implement a 3D printed fluidic port for reagent delivery which enables consistent replenishment of reagent reservoirs. In addition, we have developed a TEC based, closed-loop temperature control system for our DMF platform, providing the necessary thermal requirements for a variety of biological assays. Both of these systems serve to improve the “world-to-chip” interface tool-box for DMF. To demonstrate these principles, we have performed a bacterial transformation protocol on DMF. We report a significant improvement in transformation efficiency on our DMF platform while implementing our reagent delivery and temperature control systems. Furthermore, we demonstrate the utility of our system with an enzymatic assay to show how our reagent delivery

system improves the reproducibility of droplet dispensing on device while performing an enzymatic assay on-chip. Since this is the first reagent delivery system integrated with closed-loop temperature control, we propose that this innovation may represent an important step forward for digital microfluidics (and possibly other microfluidic platforms), making it an attractive platform for a variety of biological and chemical applications.

■ MATERIALS AND METHODS

Reagents and Materials. All general-use reagents were purchased from Sigma, unless specified otherwise. *E. coli* DH5 α and pET16b vectors were generously donated by Dr. Vincent Martin and pFAB4876 plasmids were generously donated by the Joint BioEnergy Institute (see Table S1 and Figure S1 for plasmid maps). Mini-prep kits (cat no. BS413) were purchased from BioBasic (Amherst, NY).

DMF device fabrication reagents and supplies included chromium with S1811 photoresist on glass slides from Telic (Valencia, CA), indium tin oxide (ITO)-coated glass slides, $R_S = 15\text{--}25 \Omega$ (cat no. CG-61IN-S207, Delta Technologies, Loveland CO), FluoroPel PFC1601 V from Cytonix LLC (Beltsville, MD), MF-321 positive photoresist developer from Rohm and Haas (Marlborough, MA), CR-4 chromium etchant from OM Group (Cleveland, OH), and AZ-300T photoresist stripper from AZ Electronic Materials (Somerville, NJ). TEC/Peltier module from TE technology (Traverse City, MI, USA). For 3D printing, polylactic acid (PLA) material were purchased from 3Dshop (Mississauga, ON, Canada). 3-(Trimethoxysilyl) propyl methacrylate solution for silanization from Sigma (cat no. 440159). Parylene C pellets were purchased from Specialty Coating Systems (Indianapolis, IN).

Designing, Fabrication, and Operation of the 3D Printed Well. 3D printed wells were designed using Fusion 360 3D CAD/CAM design software (Autodesk, CA United States). The design was printed using the Ultimaker 2+ extended (Shop3D, Mississauga, ON, Canada). All cylindrical wells were printed on polylactic acid (PLA) with an outer

diameter of 8 mm and with a height of 45 mm and a 1 mm diameter hole (see Figure S2). For 3D printing, STL files were generated and converted to gcode format using Acura 3D conversion with the following settings: nozzle, 0.4 mm; material, PLA; profile, high quality. In the print setup settings, the recommended button was checked, the infill parameter was checked as “Dense” and the helper parameter checked as “Print Build Plate Adhesion and Print Support Structure”.

To use the well as a reagent delivery system, the well was aligned directly to the drilled hole on the ITO top plate which we call “ITO-well-DMF” configuration (Figure S3). Approximately, 400 μL of fluid was pipetted into the well and a 3D printed screw was used to control the delivery of the fluids into the reservoir on device. The device consisted of at least two reservoirs—a main reservoir for active dispensing of a unit droplet and an ancillary reservoir for refilling the main reservoir. The well was aligned to the center of the ancillary reservoir. The operations of refilling the main reservoir would proceed in the following four steps: (1) liquid from the 3D printed well was delivered to the ancillary reservoir using the screw via rotation action, (2) a liquid neck from the ancillary reservoir is actuated to the main reservoir, (3) the volume in the main reservoir is measured via impedance by applying 160 V_{RMS} to the electrode (see circuit Figure S4a and calibration curve Figure S4b), and (4) when the volume in the main reservoir reached 7 μL , the main and ancillary reservoirs are activated to initiate a splitting operation (i.e., breaking off the liquid neck between the two reservoirs). These four steps for refilling a reservoir is repeated for every droplet being actively dispensed from the main reservoir. For dispensing experiments on ITO–DMF (i.e., no well on the top plate) and ITO-well-DMF configurations, droplets were dispensed from the main reservoir and the reservoir and dispensed droplet volumes were measured by impedance (Figure S4).

TEC Design, Operation, and Simulation. A 20 \times 40 mm TEC (TE technology INC, Texas, USA) was integrated below the DMF device that was used to provide cooling (4 $^{\circ}\text{C}$) and heating (42 $^{\circ}\text{C}$) temperatures for procedures related to on-chip transformation. The TEC was integrated into a 3D printed module with four 3D printed screws that can be interfaced with the DMF device (Figure 1). A 20 \times 40 \times 5 mm aluminum heat block with a 1.5 mm drilled hole at the center was situated between the TEC and the DMF chip. The control hardware circuit for changing the temperature consisted of an Arduino microcontroller (Arduino Uno, Italy), a driver motor (consisting of a two half-bridge driver chip and a low resistance N-channel MOSFET) (Amazon, Mississauga, ON, Canada), and a resistance temperature detector (Building Automation Products, Inc., Gays Mills, WS) that was placed inside a hole of the aluminum heat block. The hole was filled and sealed with thermopaste (GC electronics, Rockford, IL) to secure the temperature detector in place. Finally, the bottom of the aluminum heat block consisted of a 12 V DC cooling fan used to dissipate the excess heat produced by the TEC while supplying a temperature of 4 $^{\circ}\text{C}$. For open-loop control, the TEC was connected to a DC power supply through a MOSFET dual H-bridge driver. The driving current was controlled by an Arduino Uno microcontroller programmed by the user. Generally, the TEC was set to operate in 4 $^{\circ}\text{C}$ for 60 s, then was rapidly increased to 42 $^{\circ}\text{C}$ for 60 s followed by a decrease to 4 $^{\circ}\text{C}$ for 120 s.

For closed-loop control, the temperature of the system was stabilized by a negative control-loop feedback system via the

microcontroller. A proportional-integral-derivative (PID) based software code (see Supporting Information for simulation modules) was written in Matlab/Simulink (Mathworks, MA USA). Simulations of the temperature control were executed by changing rise time, over shoot, settling-time, and steady-state error values as shown in eq 1

$$u(t) = K_p e(t) + K_i \int_0^t e(t') dt' + K_d \frac{d e(t)}{dt} \quad (1)$$

where K_p , K_i , and K_d represent gain coefficients for the proportional, integral, and derivative terms respectively, $e(t)$ represents the error between the setpoint value and the sensor measured value parameter, and $u(t)$ was a controller output. In the plant simulations, the TEC was modeled as a thermodynamic system.²¹ The thermodynamic model was split into five main energy processes: thermal conduction, Joule heating, the Peltier cooling/heating effect, the Seebeck effect, and the heat transfer effects. These processes were modeled by four equations (see Table S2), and parameters were taken from the manufacturer data sheet.

Microscale Bacterial (Co-)Transformation. Prior to the experiment, the competent *E. coli* cells were thawed on ice for 10 min. Plasmid DNA (pFAB4876 and pSB1C3) was diluted to a concentration of 1 $\mu\text{g}/\mu\text{L}$. CaCl_2 stock was prepared at 150 mM to maintain final concentration of transformation solution on chip at 75 mM of CaCl_2 . For on-chip transformation, two TECs were attached to the bottom of the DMF chip that provided two controllable thermal zones (4 and 42 $^{\circ}\text{C}$) and all reagents were initially pipetted to the cold region on the chip.

For ITO–DMF configuration, 7 μL of each reagent including competent cells, pFAB4876, pSB1C3, and CaCl_2 were pipetted into the corresponding reservoir (Figure S5a for device layout). A premade sequence code which was using our in-house software was executed to apply a voltage of 160 V_{rms} at 15 kHz frequency to dispense a 1 μL droplet from the reservoir. Dispensed droplets (1 μL each) containing the DNA plasmid, *E. coli* cells in LB media and CaCl_2 were merged together on the chip in an equal volume ratio for single (or co-) transformation experiments. After merging and mixing, a heat shock protocol was applied, which consisted of 60 s at 42 $^{\circ}\text{C}$, followed by 3 min at 4 $^{\circ}\text{C}$. The solution was taken out by pipette and placed into a micro centrifuge tube. 100 μL of fresh LB were added to the mixture and then the tube was placed at the incubator at 37 $^{\circ}\text{C}$, 220 rpm for 1 h recovery. The transformed cells were plated on an agar plate with kanamycin (50 $\mu\text{g}/\text{mL}$) or kanamycin and chloroamphenicol (35 $\mu\text{g}/\text{mL}$) antibiotic selection overnight for single and co-transformation studies, respectively. Three replicates were conducted in parallel on the same device.

For ITO-well-DMF configuration, 400 μL of cells were added to the 3D printed well (instead of directly in a reservoir) and 7 μL of the DNA plasmids and CaCl_2 were added directly to the reservoirs on chip. The procedures, followed the ITO-well transformation protocol, with an additional four steps to refill the main reservoir that contained cells. Briefly, to refill the reservoir, the solution containing cells were delivered to the ancillary reservoir by rotating the screw to descend further into the 3D printed well to push the solution from the well to the ancillary reservoir. Next, the fluid was actuated from the ancillary reservoir to form a liquid neck, which was combined with the liquid in the main reservoir. A splitting step occurred to break off the liquid neck after filling the main reservoir to a

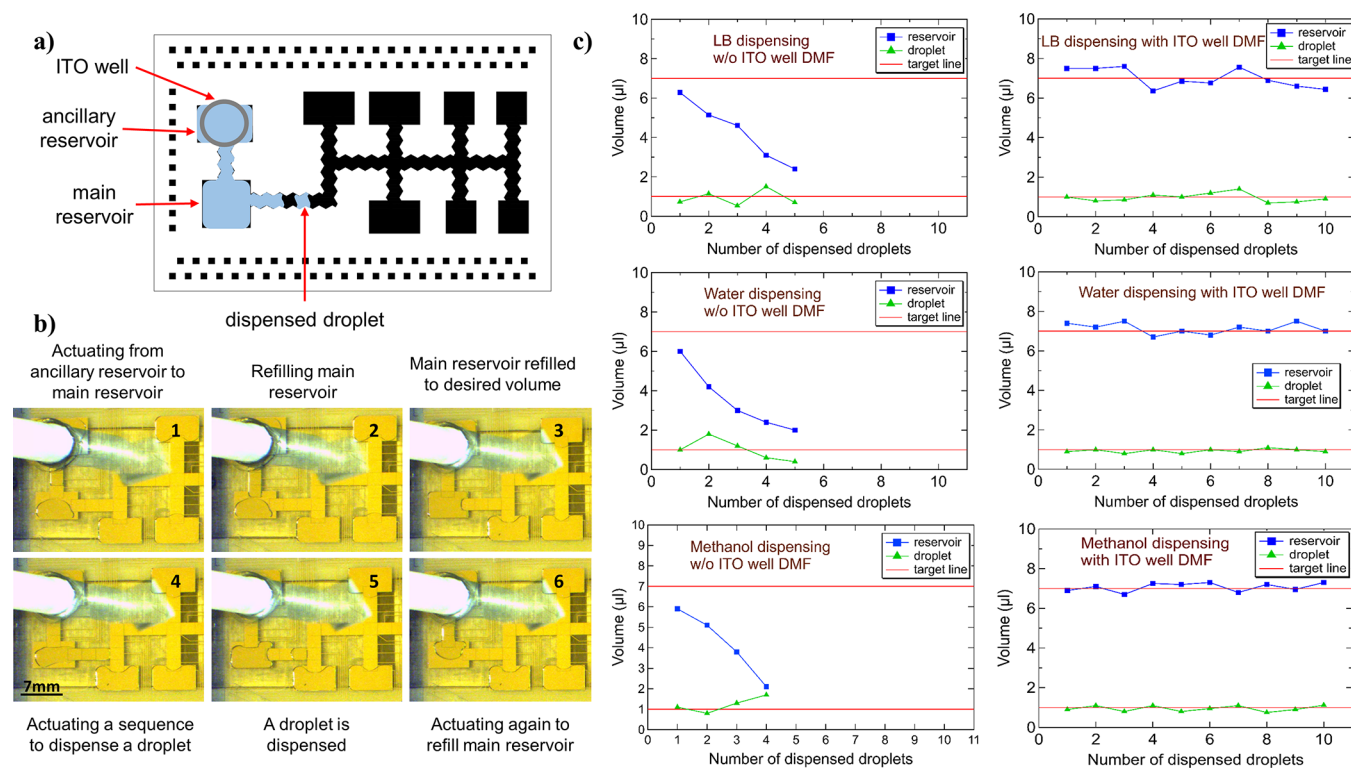


Figure 2. Reagent delivery system. (a) A schematic of a DMF device used in this study showing the alignment of the well with respect to the reservoir. Two reservoirs are depicted on the device: an ancillary and a main reservoir. The ancillary reservoir is aligned with the 3D printed well for reagent delivery. (b) A series of images from a movie to show the operation of the 3D printed well. (c) Results showing droplet dispensing using with and without the reagent delivery system for three liquids with varying viscosities: water, methanol, and LB media (with 0.05% Pluronic F-68).

desired volume of $7 \mu\text{L}$ (which was measured by impedance). Three parallel replicate measurements were performed on one device.

Enzymatic Endoglucanase Assay. The endoglucanase enzyme assay was carried out on one of the two configurations, ITO–DMF and ITO–well–DMF, and at room temperature or $30 \text{ }^\circ\text{C}$. For the $30 \text{ }^\circ\text{C}$ condition, the TEC was integrated below the assay areas and a closed-loop PID control was enabled to maintain a steady-state temperature. On the ITO–DMF configuration, a unit droplet of enzyme solution ($\sim 1 \mu\text{L}$) was dispensed into one of three assay areas on the device (see Figure S5b for the device layout) using a voltage of $160 V_{\text{RMS}}$ at 15 kHz . A substrate solution containing $40 \mu\text{M}$ 4-methylumbelliferyl β -D-cellobioside (MUC) in buffer (50 mM sodium-phosphate, $\text{pH } 7.0$) was dispensed from the reservoir and stored in an assay area. A second unit droplet of substrate solution was dispensed and serially diluted to 20 and $10 \mu\text{M}$ MUC droplets with buffer solution by mixing and splitting droplets. Two droplets containing 20 and $10 \mu\text{M}$ MUC were then individually stored in an assay area. To start the reaction, all three substrate-containing droplets were simultaneously mixed with the enzyme droplets in the assay areas (if required, the TEC was activated). After 30 min of incubation, a unit droplet of quenching solution (0.3 M glycine-NaOH, $\text{pH } 11.0$) was mixed with each reaction droplet in the assay area. On the ITO–well–DMF configuration, the same droplet operations were carried out, except that the well was used to replenish the main reservoir that contained enzyme after actively dispensing an unit droplet. After the assay, the device was placed on top of a 96-well plate and into a CLARIOStar plate reader (BMG Labtech, Ortenberg, Germany) to measure 4-methylumbelliferone (MUF) fluo-

rescence at 449 nm with 368 nm excitation. The fluorescence intensity was measured by using the well-scanning function (scan matrix = 15×15 , scan diameter = 6 mm , focal height = 4.0 mm , and gain = 1180), and the maximum fluorescence intensity value for each droplet was recorded for analysis. Each assay was repeated three times. All solutions used on the device contained 0.05% F-68 Pluronic additive.

RESULTS AND DISCUSSION

Integration of “World-to-Chip” Interfaces for Digital Microfluidics. We have integrated two world-to-chip interfaces for digital microfluidics, namely, integrating reagent delivery and temperature control systems. The new system, as shown in Figure 1a, is formed by 3D printing a bottom holder used to interface a $50 \times 75 \text{ mm}$ device, a thermoelectric cooler, a temperature sensor, and an aluminum heat block. A top 3D printed cover (shown in blue) is mated to the bottom holder with four fitting screws (shown in white) and holds in-place the pogopin holder and the device. The addition of the top cover with the fitting screws enabled tight contact of the pogopin board to the device. A top view of the device is shown in Figure 1b, as depicted, the digital microfluidic device consists of electrodes and each electrode is wired to a contact pad. The array of contact pads on the side of the device is connected to the pogopin board (which is interfaced with the automation system; see refs 5, 19, and 20 for a description). Devices are assembled with the top-plate (with or without well) and droplets are manipulated on the DMF device by applying an AC field between the top and bottom plates. Temperature control of the device is managed by the TEC module (i.e., Peltier module), which can be positioned underneath the

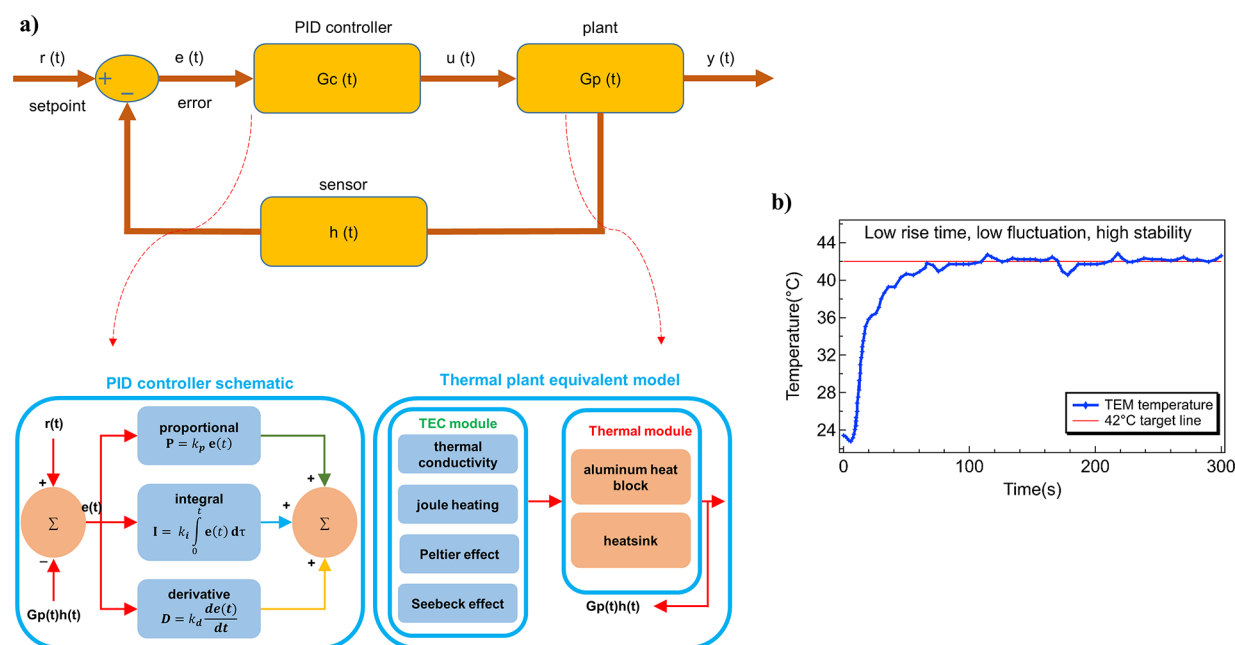


Figure 3. Thermoelectric cooler (TEC). (a) Block diagram showing the closed-loop temperature model. The model includes the PID control with a thermodynamically modeled plant design which include electrical, Peltier and thermal effects. (b) Simulation results showing optimal K_p , K_i , and K_d constants for a target temperature of 42 °C.

device with a temperature sensor for closed-loop control. Furthermore, a reagent well is attached to the top ITO plate to refill the reservoir and to dispense reproducible droplets (Figure 1b). Both of these world-to-chip interfaces represent a significant advance over the previous DMF device configurations, which do not include reagent delivery to reservoirs with refilling of the reservoirs on the device or a closed-loop control scheme for the TEC (see Table S3 comparing current “world-to-chip” DMF work and our work).^{22,23}

In current digital microfluidic systems, reagent delivery have been alleviated by the addition of reservoirs or loading pads on the device. Users manually pipette the reagents directly onto the reservoir and use automated sequences to dispense liquids from the reservoir.^{5,19,24} As shown by several groups,^{25,26} dispensing from reservoirs is not reproducible process (i.e., dispensing volumes have high variability). Current solutions to alleviate the variability in the dispensing process is to integrate capacitive²⁶ or image-based feedback²⁰ control which can measure droplet volume via impedance or image-based algorithms, respectively. In this work, we refill the reservoir after every dispensing action with the hypothesis that refilling the reservoir will reduce the variability in the dispensing process. As shown in Figure 2, the central feature of our reagent delivery design is a 3D printed cylindrical reagent well mated to the top of the ITO ground plate, which contains a drilled-hole inlet aligned to a reservoir on-chip. Using a reagent well, devices can hold larger volumes ($\sim 400 \mu\text{L}$) than a typical reservoir (which hold $\sim 1\text{--}10 \mu\text{L}$) on the chip. We call this configuration “ITO-well-DMF” and the liquid in the 3D printed well refills the reservoir on-chip by rotating the 3D printed screw further down the well. The refilling process is repeated when there has been reduction in liquid volume on the reservoir. In optimizing the design and alignment of the reagent well, the well is capable to (1) continuously deliver reagents to the reservoir that will allow repetitive droplet dispensing and (2) enable reproducible droplet dispensing from the reservoir. We observe that reliable refilling and

reproducible dispensing requires two reservoirs on-chip. From our experiments, if the well is directly overlapping the main reservoir (or partial overlap as suggested from a previous study²⁷), the fluid from the well is not confined to the reservoir and will spread elsewhere on the device. In this configuration, the main reservoir is frequently overfilled ($>7 \mu\text{L}$), which can cause significant difficulties in dispensing unit droplets. A motorized component to automatically deliver the liquids would alleviate this,^{15,28,29} but here, we added an ancillary (i.e., secondary) reservoir to refill the main reservoir and an impedance circuit to measure the volume (Figure 2a for device design and Figure S4a for impedance circuit). We observe that the addition of an ancillary reservoir facilitated easy refilling without any external motors or pumps. The process of reagent delivery follows four steps (Figure 2b): (1) liquid from the 3D printed well is delivered to the ancillary reservoir (by rotating the screw), and (2) liquid from the ancillary reservoir is “pulled” out of the reservoir and forms a liquid neck. The liquid neck merges with the liquid in the main reservoir, (3) when the volume in the main reservoir reaches a target volume of $7 \mu\text{L}$ (i.e., $V_{\text{read}} = 12.9 \text{ V}$; Figure S4b) in the main reservoir, the liquid neck is broken off by actuating the ancillary and main reservoir. With only the main reservoir (i.e., without an ancillary reservoir), a significant amount of trial-and-error was required to reach the target reservoir volume. The excess time to refill the main reservoir to the target volume typically “fouls” the surface of device which prevents droplets to be actuated in that area. With the ancillary reservoir, a systematic process is introduced (i.e., without trial-and-error) which minimized the biofouling on the surface of the device and allowed further droplet manipulation.

After the refilling process, we have tested our hypothesis of refilling reservoirs to improve the reproducibility of the dispensing process from the reservoir on-chip. As shown in Figure 2c, are six graphs showing the utility of the reagent well and the precision of dispensing using the ITO-well-DMF and ITO-DMF configurations for three types of liquids ranging in

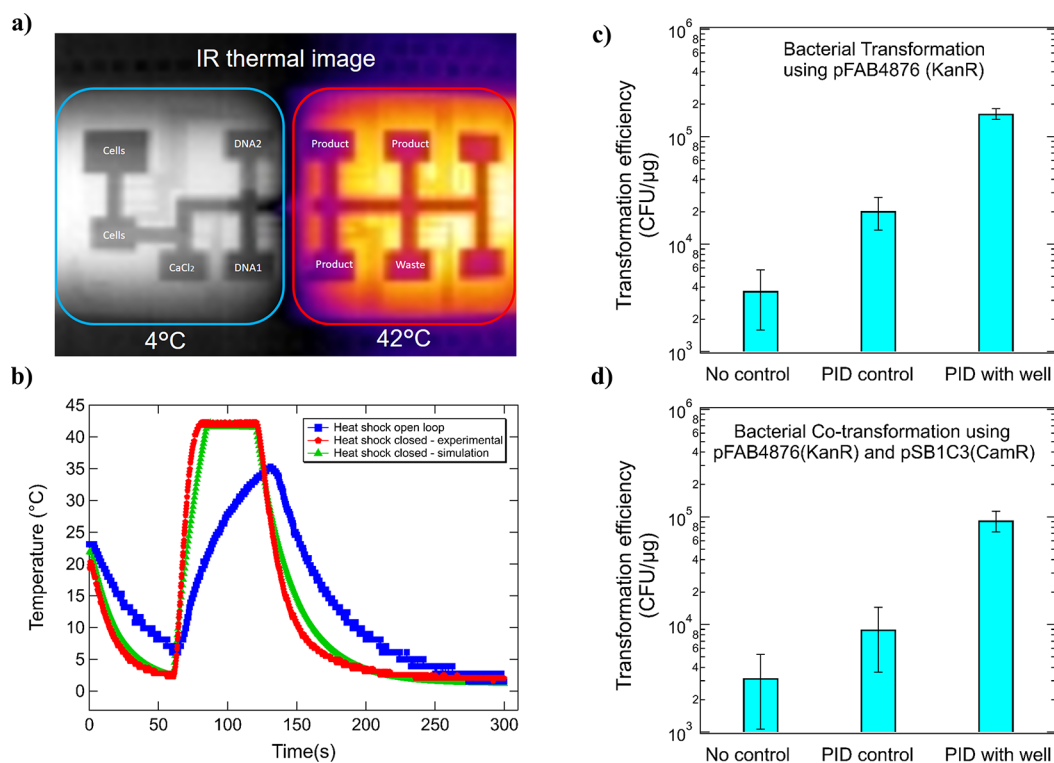


Figure 4. Application 1: Bacterial transformation. (a) An infrared image showing the heating (42 °C) and cooling regions (4 °C) on a DMF device used for transformation. (b) A comparison between simulated and experimental results for open- and closed-loop control. The transformation efficiency for (c) single- and (d) co-transformation experiments. For each set of transformation experiments, three conditions were tested: open-loop temperature control using ITO–DMF configuration and closed-loop temperature control using ITO–DMF and ITO–well–DMF configurations. Error bars are ± 1 SD from three replicate measurements.

viscosity (LB media, water, and methanol). In the ITO–DMF configuration, droplets are repeatedly dispensed from the main reservoir until it was not possible to dispense any more droplets. In our experiments, the maximum number of droplets dispensed with an initial reservoir volume of 7 μL is five droplets with a target volume of ~ 1 μL . In the ITO–well–DMF configuration, the main reservoir has been refilled after a droplet is dispensed from the reservoir. Two key results are shown from these graphs: (1) the ITO–well–DMF configuration (i.e., refilling the main reservoir) allowed continuous dispensing—we dispensed 10 droplets (compared to only 5 droplets without the well) to show the capabilities of repetitive dispensing, but it can be potentially used to dispense more droplets. (2) The precision of the dispensed droplets in the ITO–well–DMF configuration (RSD = 11.62%, 16.78%, 15.32% for LB, water, methanol, respectively) was higher than the precision in the ITO–DMF configuration (RSD = 19.61%, 49.29%, 35.41% for LB, water, methanol, respectively), which demonstrates the reproducibility of using the reagent well (and verifying our hypothesis). There are a number of factors that suggest that there is a fundamental change occurring on the device (e.g., dielectric degradation, contact angle saturation, etc.) that can change the dispensed droplet volume.²⁵ These are inevitable changes on the device and integrating a reagent well is a simple solution (to our knowledge) to refill reservoirs and to ensure reproducible droplet dispensing on-chip.

A second world-to-chip interface that plays an important role is the control of temperature on chip. There are numerous papers that have discussed the integration of microheaters (i.e., TEC elements) to establish a uniform or gradient temperatures

in a given region on a microfluidic device.^{8,30–32} However, in current microfluidic studies, the parameters used for the TEC are optimized for their own biological or chemical application. There has not been a fully modeled and characterized TEC control system that allows for a quick analysis, design, and optimization. In fact, a significant amount of trial-and-error is required to optimize the control-loop parameters and design. A model-based approach can reduce the time and the number of iterations to tune the control-loop parameters to meet the demand specifications on-chip. The simulation model that we have developed and used is described in Figure 3a (and Supporting Information). The temperature setpoint is the value subtracted from the measured value (feedback) from the temperature sensor that is located in the heat-block. The difference (the error) is the input to the PID controller. The PID controller calculates the next-step output value by using the error value with a set of parameters K_p , K_i , and K_d (for proportional, integral, and derivative control respectively). The output is connected to the plant thermoelectric module (which is modeled by two main effects: thermal and Peltier). The output of the plant is read by the temperature sensor and returned to the input. As a first test, we verified the authenticity of the model to check the robustness, stability, and accuracy of the closed-loop system. For that reason, we chose three different scenarios to numerically simulate the target temperature of 42 °C. Using parameters $K_p = 15$, $K_i = 1.2$, and $K_d = 0.5$ shows the optimal behavior in terms of the demands (Figure 3b, see Figure S6ab for other simulated scenarios), that is, fast rise time, low fluctuation, and high stability at the target temperature of 42 °C. The simulation shows that parameters K_p and K_i are sensitive to changing the stability and overshoot

Table 1. Comparison of Transformation Efficiency for Three Different Methodologies: No Control, PID Control, and PID Control with Well

transformation type	experiment	plasmid		plasmid mass (ng)		antibiotic selection		transformation efficiency (CFU/ μ g DNA)	standard error ($n = 3$)
		A	B	A	B	Kan	Cam		
single	no control	n/a	pSB1C3-RFP ^a	n/a	100	–	+	4.93×10^4	1.82×10^4
	no control	pFab4876	n/a	100	n/a	+	–	3.67×10^3	1.20×10^3
	PID control	pFab4876	n/a	100	n/a	+	–	2.03×10^4	3.93×10^3
	PID control with well	pFab4876	n/a	100	n/a	+	–	1.48×10^5	1.36×10^4
co-	no control	pFab487S	pSB1C3-RFP ^a	100	100	+	+	3.17×10^3	2.42×10^3
	PID control	pFab4876	pSB1C3-RFP ^a	100	100	+	+	9.00×10^3	3.12×10^3
	PID control with well	pFab4876	pSB1C3-RFP ^a	100	100	+	+	9.27×10^4	1.17×10^4

^aRFP gene is BBa_J04450 insert from the IGENE part registry.

of the target. This observation is expected since increasing the proportional gain (K_p) will have the effect of reducing the rise time while the steady state error can be eliminated by introducing some element of integral control (K_i). Given the simplicity of our model, this will allow users who are not familiar with control theory to implement closed-loop temperature control and integrate with reagent delivery control for digital microfluidics.

Applications of “World-to-Chip” Interfaces. *Application 1: Bacterial Transformation.* To evaluate the functionality of the world-to-chip interfaces, we have conducted a bacterial transformation study on our digital microfluidic device. Bacterial transformation involves the insertion of plasmid DNA into *E. coli* (or some microbe) using a heat shock (or electric-field) based methods. Microbial plasmid-based systems can aid in the understanding of protein functions and interactions within the cell, as well as serve as a storage system for genetic components. There has been much interest in automating the transformation procedure using digital microfluidics (or a derivative thereof)^{7,33,34} since fields like synthetic biology typically requires the optimization of metabolic pathways³⁵ or building logic gated systems³⁶ consisting of many genetic elements that can be difficult to manipulate if manually performed. Here, we contribute a closed-loop temperature control and a reagent delivery system that is not present in these studies.

To perform transformation with our integrated world-to-chip interfaces, we designed a microfluidic device (see Figure S5a) that is capable of automated transformation using heat-shock protocols. The device consists of four reservoirs that holds droplets of cells, LB media, CaCl₂ solution, and the plasmid coding for a fluorescent protein. Two new features (compared to other DMF and transformation studies) have been added to this configuration: (1) a 3D printed well that is used to automate reagent delivery to the reservoirs and (2) the closed-loop PID control of the TEC. We also integrate the TEC module below our DMF device to provide a region with controllable thermal zones (Figure 4a). The canonical *E. coli* heat shock protocol requires temperature flux between 4 and 42 °C and we have programmed the TEC to optimally control the fluctuation between these temperatures. We have implemented an experiment to determine if the module is capable of reaching the desired temperatures. As shown in Figure 4b, the open loop control of the TEC is not capable of moving between desired temperatures of 4 and 42 °C within the desired time of 1 min. However, with the closed loop PID control system, we observe that temperatures can quickly rise

to 42 °C at a rate of 2.1 °C/s and drop to 4 °C at a rate of 1.01 °C/s (which was also verified via simulation). The closed loop PID system is important since it has been shown that temperature fluctuations affect transformation efficiency for some species of bacteria in which the length of incubation time at these temperatures can affect the uptake of the donor DNA.^{37,38} Next, we have tested the closed-loop control system by experimentally transforming chemically competent *DH5 α* *E. coli* cells with expressing *GFP* from the pFAB4876 plasmid. As shown in Figure 4c and Table 1, the PID control TEC gave rise to an efficiency of 2.03×10^4 colonies forming units per μ g of DNA (CFU/ μ g). This was significantly ($P = 0.041$ at 95% confidence) higher than the open-loop controlled transformation (3.67×10^3 CFU/ μ g). As expected, the temperature control for on-chip transformation plays a significant role on the transformation efficiency (as observed in other studies⁸). In addition, we hypothesize that with that the reagent well delivery system, we will obtain higher transformation efficiency due to dispensing droplets at more precise volumes. Our data validated our hypothesis—for example, in three trials of conducting bacterial transformation on-chip using the reagent delivery system and with closed loop control improved the transformation by 7-fold ($p = 1.48 \times 10^5$ CFU/ μ g, $p = 0.007$) compared to the closed-loop control and with usual dispensing techniques (i.e., no refilling the reservoir after one dispensing action). A possible explanation for this increase is that variable dispensing volumes can create variability in final DNA concentrations, pH of the solution, CaCl₂ treatment, and nutrient concentration in which all of these factors can affect overall transformation efficiencies.^{39–42} We also have conducted a third experiment to measure the efficiency for transforming two DNA plasmids (i.e., co-transformation). We are motivated by their widespread use in gene-editing⁴³ or metabolic engineering⁴⁴ that require transformation of multiple plasmids for the expression of multiple genes. We hypothesize that similar trends are observed for these experiments as the single transformation experiments. As shown in Figure 4d and Table 1, the trends confirm to be similar such that the integration of both world-to-chip interfaces significantly improved the efficiency ($p = 0.001$). We also have evaluated the differences between single and co-transformation (Table 1) and single transformation are generally higher in efficiency regardless of the methodology used for liquid delivery and temperature control. Overall, we have demonstrated the need for the world-to-chip interfaces for digital microfluidics and propose that method described

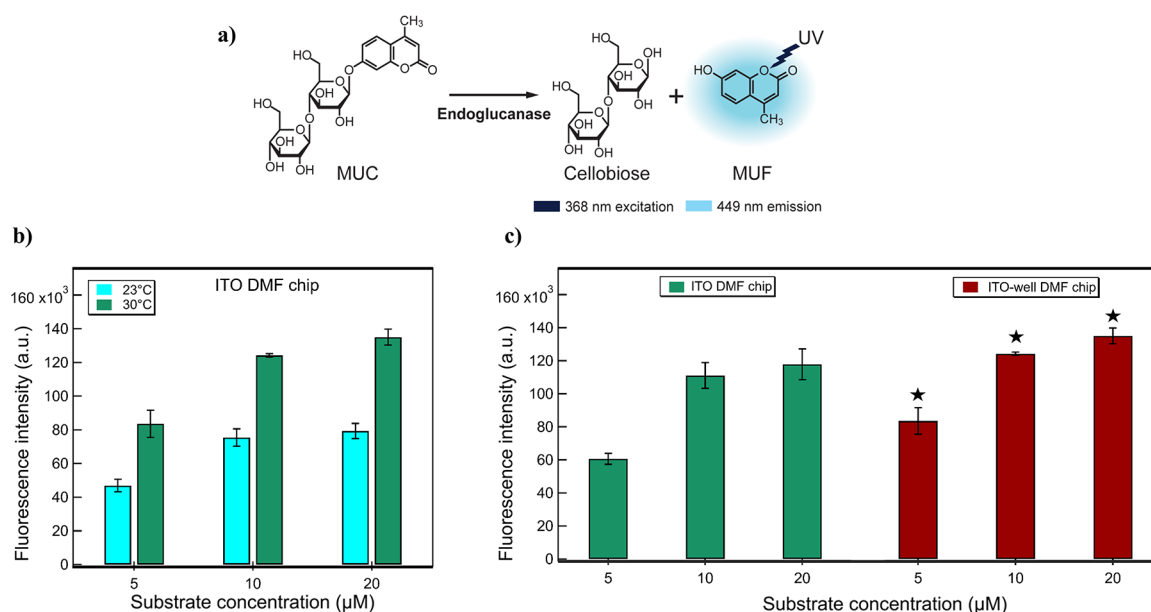


Figure 5. Application 2: Enzymatic assay. (a) Schematic showing the chemical scheme of the enzymatic assay. (b) Data generated on-chip showing the effects of temperature on the enzymatic assay at two different temperatures (23 and 30 °C). (c) Experimental accuracy for ITO-DMF and ITO-well-DMF driven enzymatic assays. The enzymatic assay was evaluated for three substrate concentrations (5, 10, and 20 μ M) with the enzyme concentration remaining constant. All samples were analyzed in triplicates with error bars showing ± 1 SD.

here would be uniquely suited for future experiments involving bacterial transformation.

Application 2: Enzymatic Endoglucanase Assays. As a second demonstration of an application for our world-to-chip interfaces integrated with digital microfluidics, we explore the implementation of enzymatic assays. Enzymatic assays are often used to measure the activity of produced proteins and are vital to understanding enzyme kinetics and inhibition. The enzyme kinetics provides crucial information on the mechanism of the enzyme and on the interactions of the enzymes with substrates, inhibitors, drugs, etc. One of the fundamental applications of DMF is the implementation of enzymatic reactions.^{20,45–48} The protocol typically consists of precise metering of reactants by dispensing droplets from reservoirs and merging and mixing to create a droplet that represents the microreactor. The microreactors on the DMF device have been analyzed using integrated in-line detectors^{19,49,50} or with offline detectors (e.g., fluorescence-based plate readers).^{5,14,51} However, most enzymatic assays on DMF are either performed at room temperature or without refilling of reservoirs for dispensing droplets.^{45,52,53} These corresponding factors give rise to two limitations: (1) prevents the study of most industrial-based and thermoresistant enzymes, which are active at higher temperatures (>25 °C), and (2) prevents the study of different conditions on the device that requires droplets (containing substrate enzyme, or buffer) to be dispensed multiple times. These limitations motivate the development of our world-to-chip for digital microfluidics for the implementation of enzymatic assays that require heating and testing of multiple conditions in parallel.

Here, we report an enzymatic reaction that involves cellulase-based enzymes that are involved in the degradation of biomass into sugar that are useful for biofuel production.⁵⁴ Specifically, we have tested an endoglucanase (which are optimal at higher temperatures) that is typically used to catalyze the hydrolysis of the (1,4)-glycosidic bonds.⁵⁵ Droplets containing the 4-methylumbelliferyl β -D-cellobioside

(MUC; substrate) and the endoglucanase enzyme have been mixed and incubated for 30 min using the same DMF device as described in the [Methods](#) section. After incubating, the droplets have been analyzed via fluorescence. [Figure 5a](#) shows the chemical scheme of the assay which consists of using MUC in which the endoglucanase cleaves the β -(1,4) bond to give a cellobiose and a methylumbelliferone fluorescence product. Using this chemical scheme, we have tested the enzymatic activity of the endoglucanase using the 3D printed well for refilling of the reservoirs on the device to enable reproducible droplet dispensing of the enzyme and the closed-loop TEC to perform the assay at elevated temperatures (30 °C). The fluorescence output (i.e., the measure for enzyme activity) as a function of three substrate concentrations (5, 10, 20 μ M) at two temperatures (23 and 30 °C), illustrated in [Figure 5b](#), show the key trend is reproduced, that is, a higher temperature lead to higher output fluorescence compared to room temperature experiments.

In a second assay, we performed the enzymatic assay with and without the reagent delivery system and with the closed-loop TEC system set to a target temperature of 30 °C. [Figure 5c](#) shows the fluorescence output for each substrate concentration with and without the reagent delivery system. As shown, the fluorescence is significantly higher (ANOVA two-way test, $P < 0.05$) for experiments with the reagent delivery system. A potential cause for this difference between the data are changes in the droplet volumes. There are studies that show small changes in volume can lead to changes in the pH, salt, and detergent concentrations, which can reduce the activity and stability of thermophilic enzymes by 20–30%.^{56,57} In the future, given the widespread interest of automating enzymatic assays on DMF, we propose that the world-to-chip techniques reported here, in which reagent delivery and refilling and integration of closed-loop temperature control will be useful for other types of enzymatic-based or other types of biological assays.

CONCLUSIONS

We have developed two interfaces, namely a reagent delivery system and a closed-loop heating/cooling module, that can be added to the “world-to-chip” tool-box for digital microfluidic systems. The reagent delivery system consists of a 3D printed well integrated to the top-plate of the DMF device. The reagent well is fitted with a threaded screw that is used to deliver liquid directly to an on-chip reservoir. The refilling process of the liquid in the reservoir follows several digital microfluidic actuation sequences and an impedance measurement to measure target volume in the reservoir. We also have incorporated a closed-loop thermal/cooling TEC to rapidly control the temperature on the device. To understand and to verify the experimental results of the TEC, we have created a closed-loop model to simulate the temperatures on the device. Finally, we have applied our world-to-chip interfaces to two widely adopted applications: bacterial transformation and enzymatic assays. Both applications show the requirement for world-to-chip interfaces and demonstrate the potential in moving toward a customizable and automated benchtop digital microfluidic system

ASSOCIATED CONTENT

Supporting Information

The Supporting Information is available free of charge on the ACS Publications website at DOI: [10.1021/acs.analchem.8b05754](https://doi.org/10.1021/acs.analchem.8b05754).

Microfluidic device fabrication and operation, competent cell preparation, cloning and protein expression, plasmid map, design and configuration of the 3D printed well, reagent delivery interface for digital microfluidic devices, impedance measurement circuit to measure fluid volume on the device, DMF design layout, effects of closed-loop temperature control with non-optimal control parameters, description of strains and plasmids used in this study, equations and parameters used to model the closed-loop thermoelectric cooler, comparison of “world-to-chip” interfaces on DMF and our work, and thermal plant details (PDF)

AUTHOR INFORMATION

Corresponding Author

*Tel: +1-(514) 848-2424, ext 7579. E-mail: steve.shih@concordia.ca.

ORCID

Steve C. C. Shih: [0000-0003-3540-0808](https://orcid.org/0000-0003-3540-0808)

Author Contributions

E.M. and S.C.C.S. designed the experiments. E.M. designed and fabricated the DMF device and ITO-well-DMF. E.M. and J.M.P. designed the TEC setup for device integration. G.S. modeled and built the thermal simulation of the systems and wrote the software to automate and control the experiment including the real-time control-loop. E.M., J.M.P., and M.C.H. carried out the experiments on- and off-chip and analyzed the data with S.C.C.S. E.M., J.M.P., and S.C.C.S. wrote the paper. All authors reviewed the final version of the manuscript before submission.

Notes

The authors declare no competing financial interest.

ACKNOWLEDGMENTS

We thank Vincent Martin's laboratory for donating plasmids and strains and the Centre of Applied Synthetic Biology (CASB) for their technical support. We thank the Natural Sciences and Engineering Research Council (NSERC), the Fonds de Recherche Nature et technologies (FRQNT), and the Canadian Foundation of Innovation (CFI) for funding. We thank the Department of Electrical and Computer Engineering at Concordia University for FRS Funding.

REFERENCES

- (1) Laksanasopin, T.; Guo, T. W.; Nayak, S.; Sridhara, A. A.; Xie, S.; Olowookere, O. O.; Cadinu, P.; Meng, F.; Chee, N. H.; Kim, J.; et al. *Sci. Transl. Med.* **2015**, *7* (273), 273re1.
- (2) Moore, T. A.; Brodersen, P.; Young, E. W. *Anal. Chem.* **2017**, *89* (21), 11391–11398.
- (3) Kwon, S.; Cho, C. H.; Kwon, Y.; Lee, E. S.; Park, J. K. *Sci. Rep.* **2017**, *7*, 45968.
- (4) Choi, K.; Ng, A. H.; Fobel, R.; Chang-Yen, D. A.; Yarnell, L. E.; Pearson, E. L.; Oleksak, C. M.; Fischer, A. T.; Luoma, R. P.; Robinson, J. M.; et al. *Anal. Chem.* **2013**, *85* (20), 9638–9646.
- (5) Sinha, H.; Quach, A. B.; Vo, P. Q.; Shih, S. C. *Lab Chip* **2018**, *18* (15), 2300–2312.
- (6) Ng, A. H.; Dean Chamberlain, M.; Situ, H.; Lee, V.; Wheeler, A. R. *Nat. Commun.* **2015**, *6*, 7513.
- (7) Shih, S. C.; Goyal, G.; Kim, P. W.; Koutsoubelis, N.; Keasling, J. D.; Adams, P. D.; Hillson, N. J.; Singh, A. K. *ACS Synth. Biol.* **2015**, *4* (10), 1151–1164.
- (8) Gach, P. C.; Shih, S. C.; Sustarich, J.; Keasling, J. D.; Hillson, N. J.; Adams, P. D.; Singh, A. K. *ACS Synth. Biol.* **2016**, *5* (5), 426–433.
- (9) Liu, R. H.; Stremmer, M. A.; Sharp, K. V.; Olsen, M. G.; Santiago, J. G.; Adrian, R. J.; Aref, H.; Beebe, D. J. *J. Microelectromech. Syst.* **2000**, *9* (2), 190–197.
- (10) Oh, K. W.; Park, C.; Namkoong, K.; Kim, J.; Ock, K. S.; Kim, S.; Kim, Y. A.; Cho, Y. K.; Ko, C. *Lab Chip* **2005**, *5* (8), 845–850.
- (11) Maeki, M.; Yamazaki, S.; Pawate, A. S.; Ishida, A.; Tani, H.; Yamashita, K.; Sugishima, M.; Watanabe, K.; Tokeshi, M.; Kenis, P. J. A.; Miyazaki, M. *CrystEngComm* **2016**, *18* (40), 7722–7727.
- (12) Froger, A.; Hall, J. E. *J. Visualized Exp.* **2007**, No. 6, e253.
- (13) Shih, S. C.; Gach, P. C.; Sustarich, J.; Simmons, B. A.; Adams, P. D.; Singh, S.; Singh, A. K. *Lab Chip* **2015**, *15* (1), 225–36.
- (14) Yang, H.; Luk, V. N.; Abalgawad, M.; Barbulovic-Nad, I.; Wheeler, A. R. *Anal. Chem.* **2009**, *81* (3), 1061–1067.
- (15) Au, A. K.; Bhattacharjee, N.; Horowitz, L. F.; Chang, T. C.; Folch, A. *Lab Chip* **2015**, *15* (8), 1934–41.
- (16) Waheed, S.; Cabot, J. M.; Macdonald, N. P.; Lewis, T.; Guijt, R. M.; Paull, B.; Breamore, M. C. *Lab Chip* **2016**, *16* (11), 1993–2013.
- (17) Patrick, W. G.; Nielsen, A. A.; Keating, S. J.; Levy, T. J.; Wang, C.-W.; Rivera, J. J.; Mondragón-Palomino, O.; Carr, P. A.; Voigt, C. A.; Oxman, N.; et al. *PLoS One* **2015**, *10* (12), e0143636.
- (18) Gong, H.; Woolley, A. T.; Nordin, G. P. *Lab Chip* **2016**, *16* (13), 2450–8.
- (19) Husser, M. C.; Vo, P. Q. N.; Sinha, H.; Ahmadi, F.; Shih, S. C. *ACS Synth. Biol.* **2018**, *7* (3), 933–944.
- (20) Vo, P. Q.; Husser, M. C.; Ahmadi, F.; Sinha, H.; Shih, S. C. *Lab Chip* **2017**, *17* (20), 3437–3446.
- (21) Tsai, H.-L.; Lin, J.-M. *J. Electron. Mater.* **2010**, *39* (9), 2105–2111.
- (22) Shah, G. J.; Ding, H.; Sadeghi, S.; Chen, S.; Kim, C. J.; van Dam, R. M. *Lab Chip* **2013**, *13* (14), 2785–95.
- (23) Au, S. H.; Shih, S. C.; Wheeler, A. R. *Biomed. Microdevices* **2011**, *13* (1), 41–50.
- (24) Jebail, M. J.; Wheeler, A. R. *Curr. Opin. Chem. Biol.* **2010**, *14* (5), 574–81.
- (25) Elvira, K. S.; Leatherbarrow, R.; Edel, J.; deMello, A. *Biomicrofluidics* **2012**, *6* (2), 022003.
- (26) Gong, J.; et al. *Lab Chip* **2008**, *8* (6), 898–906.

- (27) Boles, D. J.; Benton, J. L.; Siew, G. J.; Levy, M. H.; Thwar, P. K.; Sandahl, M. A.; Rouse, J. L.; Perkins, L. C.; Sudarsan, A. P.; Jalili, R.; et al. *Anal. Chem.* **2011**, *83* (22), 8439–8447.
- (28) Jebrail, M. J.; Sinha, A.; Vellucci, S.; Renzi, R. F.; Ambriz, C.; Gondhalekar, C.; Schoeniger, J. S.; Patel, K. D.; Branda, S. S. *Anal. Chem.* **2014**, *86* (8), 3856–3862.
- (29) Kim, H.; Jebrail, M. J.; Sinha, A.; Bent, Z. W.; Solberg, O. D.; Williams, K. P.; Langevin, S. A.; Renzi, R. F.; Van De Vreugde, J. L.; Meagher, R. J.; et al. *PLoS One* **2013**, *8* (7), e68988.
- (30) Shilton, R. J.; Mattoli, V.; Travagliati, M.; Agostini, M.; Desii, A.; Beltram, F.; Cecchini, M. *Adv. Funct. Mater.* **2015**, *25* (37), 5895–5901.
- (31) Prakash, R.; Pabbaraju, K.; Wong, S.; Wong, A.; Tellier, R.; Kaler, K. V. *Micromachines* **2015**, *6* (1), 63–79.
- (32) Velve Casquillas, G.; Fu, C.; Le Berre, M.; Cramer, J.; Meance, S.; Plecis, A.; Baigl, D.; Greffet, J.-J.; Chen, Y.; Piel, M.; et al. *Lab Chip* **2011**, *11* (3), 484–489.
- (33) Moore, J.; Nemat-Gorgani, M.; Madison, A.; Sandahl, M.; Punnamaraju, S.; Eckhardt, A.; Pollack, M.; Vigneault, F.; Church, G.; Fair, R.; et al. *Biomicrofluidics* **2017**, *11* (1), 014110.
- (34) Madison, A. C.; Royal, M. W.; Vigneault, F.; Chen, L.; Griffin, P. B.; Horowitz, M.; Church, G. M.; Fair, R. B. *ACS Synth. Biol.* **2017**, *6* (9), 1701–1709.
- (35) Campbell, A.; Bauchart, P.; Gold, N. D.; Zhu, Y.; De Luca, V.; Martin, V. J. *ACS Synth. Biol.* **2016**, *5* (5), 405–414.
- (36) Potvin-Trottier, L.; Lord, N. D.; Vinnicombe, G.; Paulsson, J. *Nature* **2016**, *538* (7626), 514.
- (37) Khanna, M.; Stotzky, G. *Appl. Environ. Microbiol.* **1992**, *58* (6), 1930–1939.
- (38) Lacks, S. A.; Ayalew, S.; De La Campa, A. G.; Greenberg, B. *Mol. Microbiol.* **2000**, *35* (5), 1089–1098.
- (39) Rahimzadeh, M.; Sadeghizadeh, M.; Najafi, F.; Arab, S.; Mobasheri, H. *Mol. Biol. Res. Commun.* **2016**, *5* (4), 257–261.
- (40) Moore, M. E.; Lam, A.; Bhatnagar, S.; Solnick, J. V. *J. Bacteriol.* **2014**, *196* (2), 337–344.
- (41) Asif, A.; Mohsin, H.; Tanvir, R.; Rehman, Y. *Front. Microbiol.* **2017**, *8*, 2169.
- (42) Brooke, R.; Hopkins, J.; Laflamme, E.; Wark, P. *J. Exp. Microbiol. Immunol.* **2009**, *13*, 71–74.
- (43) Wang, M.; Liu, Y.; Zhang, C.; Liu, J.; Liu, X.; Wang, L.; Wang, W.; Chen, H.; Wei, C.; Ye, X.; et al. *PLoS One* **2015**, *10* (4), e0122755.
- (44) Ghosh, C.; Gupta, R.; Mukherjee, K. J. *Microb. Cell Fact.* **2012**, *11* (1), 93.
- (45) Miller, E. M.; Wheeler, A. R. *Anal. Chem.* **2008**, *80* (5), 1614–1619.
- (46) Chen, Q.; Groote, R.; Schönherr, H.; Vancso, G. J. *Chem. Soc. Rev.* **2009**, *38* (9), 2671–2683.
- (47) Ciulli, A.; Abell, C. *Curr. Opin. Biotechnol.* **2007**, *18* (6), 489–496.
- (48) Ven, K.; Safdar, S.; Dillen, A.; Lammertyn, J.; Spasic, D. *Anal. Bioanal. Chem.* **2019**, *411* (1), 205.
- (49) Srinivasan, V.; Pamula, V. K.; Fair, R. B. *Lab Chip* **2004**, *4* (4), 310–315.
- (50) Choi, K.; Mudrik, J. M.; Wheeler, A. R. *Anal. Bioanal. Chem.* **2015**, *407* (24), 7467–7475.
- (51) Luk, V. N.; Wheeler, A. R. *Anal. Chem.* **2009**, *81* (11), 4524–4530.
- (52) Srinivasan, V.; Pamula, V. K.; Fair, R. B. *Anal. Chim. Acta* **2004**, *507* (1), 145–150.
- (53) Sista, R. S.; Eckhardt, A. E.; Wang, T.; Graham, C.; Rouse, J. L.; Norton, S. M.; Srinivasan, V.; Pollack, M. G.; Tolun, A. A.; Bali, D.; et al. *Clin. Chem.* **2011**, *57* (10), 1444–51.
- (54) Peralta-Yahya, P. P.; Keasling, J. D. *Biotechnol. J.* **2010**, *5* (2), 147–162.
- (55) Gladden, J. M.; Park, J. I.; Bergmann, J.; Reyes-Ortiz, V.; D'haeseleer, P.; Quirino, B. F.; Sale, K. L.; Simmons, B. A.; Singer, S. W. *Biotechnol. Biofuels* **2014**, *7* (1), 15.
- (56) Dave, B. R.; Sudhir, A. P.; Subramanian, R. *Biotechnol. Rep.* **2015**, *6*, 85–90.
- (57) Parry, N.; Beever, D.; Owen, E.; Nerinckx, W.; Claeysens, M.; Van Beeumen, J.; Bhat, M. *Arch. Biochem. Biophys.* **2002**, *404* (2), 243–253.